JOC The Journal of Organic Chemistry

Article

pubs.acs.org/joc

Mechanistic Insights on Cooperative Asymmetric Multicatalysis Using Chiral Counterions

Garima Jindal and Raghavan B. Sunoj*

Department of Chemistry, Indian Institute of Technology Bombay, Powai, Mumbai 400076, India

Supporting Information

ABSTRACT: Cooperative multicatalytic methods are steadily gaining popularity in asymmetric catalysis. The use of chiral Brønsted acids such as phosphoric acids in conjunction with a range of transition metals has been proven to be effective in asymmetric synthesis. However, the lack of molecular-level understanding and the accompanying ambiguity on the role of the chiral species in stereoinduction continues to remain an unresolved puzzle. Herein, we intend to disclose some novel transition state models obtained through DFT(B3LYP and M06) computations for a quintessential reaction in this family, namely, palladium-catalyzed asymmetric Tsuji−Trost allylation of aldehydes. The aldehyde is activated as an enamine by the action of a secondary amine (organocatalysis), which then adds to an activated Pd-allylic species (transition metal catalysis) generated through the protonation of allyic alcohol by chiral BINOL-phosphoric acid (Brønsted acid catalysis). We aim to decipher the nature of chiral BINOL-phosphates and their role in creating a quaternary chiral carbon atom in this triple catalytic system. The study reports the first transition state model capable of rationalizing chiral counterion-induced enantioselectivity. It is found that the chiral phosphate acts as a counterion in the stereocontrolling event rather than the conventional ligand mode.

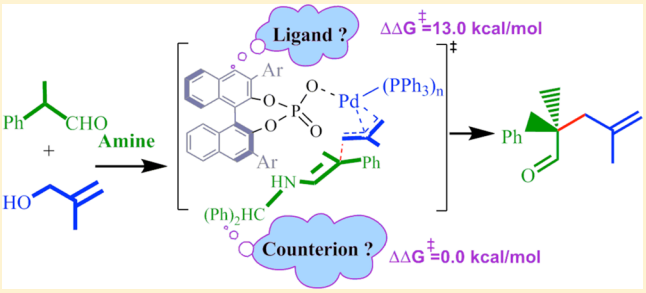

INTRODUCTION

Transition metals suitably nested into chiral ligands have long been employed in asymmetric catalysis.[1] While a gamut of such time-tested catalysts are in use, an interestingly promising class of noncovalently linked chiral motifs are becoming popular.[2] Contemporary literature also provides indications that the complementary potential of organocatalysis and transition-metal catalysis can be blended toward the design of new cooperative multicatalytic asymmetric protocols.[3]

In the past few years, convincing demonstrations on the power of noncovalently linked chiral counterions in stereo-induction have become available.[4] The chiral counterions are now pervading both organo-[5] and transition-metal catalysis.[6] In such reactions ion-pair interactions are suggested to govern the stereoselectivity. In an exquisite illustration, List and co-workers have employed this concept in a Tsuji−Trost asymmetric allylation[1d,e] toward installing a quaternary carbon stereocenter (Scheme 1).[7] Herein, the BINOL-based chiral phosphoric acid is employed as the source for transfer of chiral information. A concept termed asymmetric counteranion directed catalysis (ACDC) encompasses a group of reactions exhibiting pivotal changes with respect to the changes in the nature of counterions.[5,6] These reactions offer tunability by manupulating the chirality on Brønsted acids and amines, as well as on the ligands.[6g]

The cooperative multicatalytic asymmetric allylation reaction, as shown in Scheme 1, is an interesting example of how multiple catalysts can be made to work toward realizing a desired target molecule. The mechanism of this reaction can be envisaged to first involve the activation of the aldehyde in the form of an enamine (**a**). The allyl alcohol gets protonated by the Brønsted acid to provide an allyl cation and the chiral phosphate counterion with a concomitant removal of water. The allyl cation is further activated as a Pd-π-allyl complex (**b**). The generation of a new chiral center occurs in the ensuing allylation step, wherein **a** adds to **b**. The overall reaction therefore relies on transition-metal (Pd), organo- (enamine), and Brønsted acid (TRIP) catalysis, each of which is well-known for their independent catalytic abilities.

Though this qualitative working hypothesis appears reasonable, the key mechanistic ambiguity pertaining to the mode of catalysis prevails as to whether the phosphate counterion transfers chirality through selective H-bonding interactions[8] or by forming an ion-pair prior to the key stereocontrolling event or even acts as a ligand directly bound to the metal.[3b,4,6] The molecular insights on the potential cooperativity between the enamine, Pd, and Brønsted acid catalytic triad is not conspicuous as well. The experimental results at this stage are not fully adequate to resolve the issues of mode of catalysis as well as the factors responsible for stereoselectivity.[9] Insights into the nature of the active species as well as on the origin of chiral induction would help further the developments in this burgeoning area of cooperative asymmetric catalysis.

Received: June 13, 2014
Published: July 22, 2014

dx.doi.org/10.1021/jo501322v | J. Org. Chem. 2014, 79, 7600−7606

Scheme 1. Asymmetric Allylation of Aldehyde Cooperatively Catalyzed by Pd, Brønsted Acid, and Amine[7]

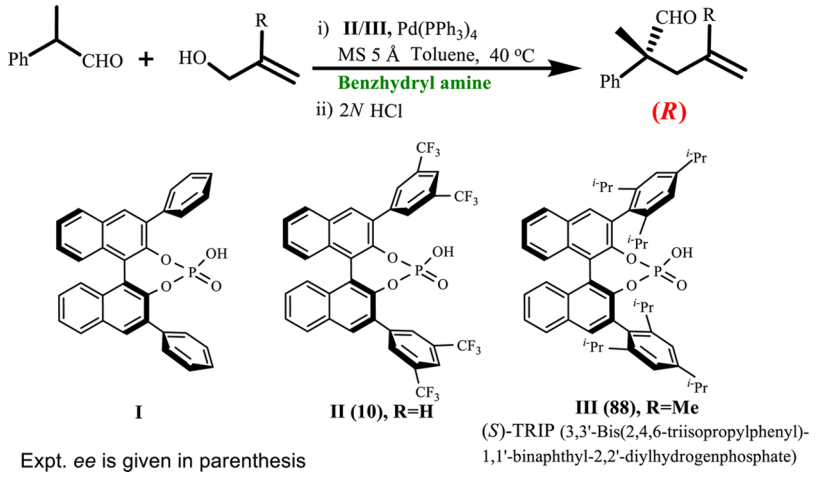

Scheme 2[a]

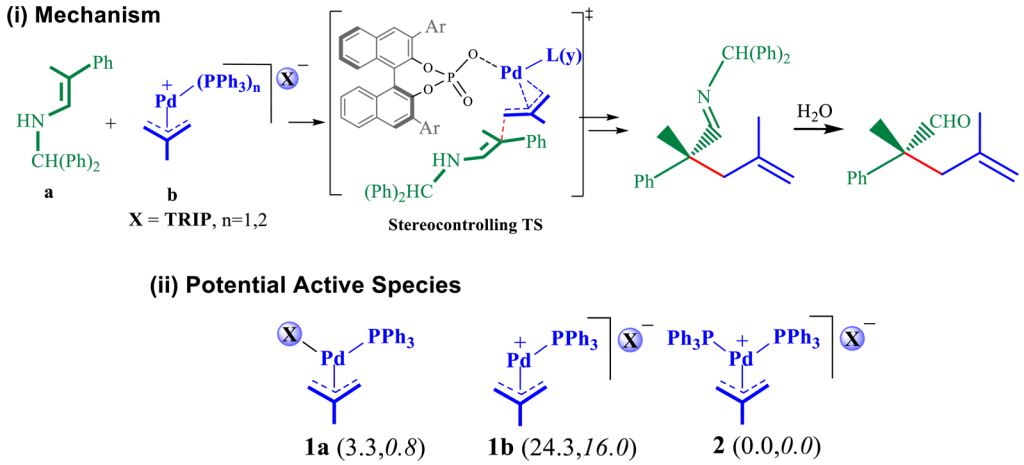

[a](i) Transition state model for the stereocontrolling C−C bond formation between π-(2-methyl)allyl-Pd and enamine derived from benzylaldehyde. (ii) Potential active species and relative Gibbs free energies (kcal/mol) in the gas phase (normal font) and in the condensed phase at the SMD(Toluene)/M06/6-31G**,LANL2DZ(Pd)//M06/6-31G**,LANL2DZ(Pd) level of theory (italics).

As part of our continued interest in asymmetric catalysis,[10] we have undertaken a DFT (M06 and B3LYP) investigation of the mechanism of the title reaction. Herein, we aim to establish (i) the nature of the catalytic species, (ii) the role of counterion in stereoinduction through transition state (TS) modeling, and (c) whether the transition metal, enamine, and the Brønsted acid act cooperatively. The discussions are presented using the M06/6-31G**,LANL2DZ(Pd) level of theory.

COMPUTATIONAL METHODS

All calculations were done using the Gaussian09 suite of quantum chemical program.[11] The hybrid density functional B3LYP was used for geometry optimization with the 6-31G** basis set for all atoms except Pd.[12] For Pd atom the LANL2DZ basis set consisting of effective core potential (ECP) and double-ζ quality valence basis set was used.[13] The stationary points were characterized by frequency calculations. The transition states were verified by the unique imaginary frequency pertaining to the desired reaction coordinate. Intrinsic reaction coordinate (IRC) calculations were carried out to ascertain the correctness of the transition states obtained.[14] The end-point geometries obtained through the IRC calculation were subjected to further geometry optimization using a more stringent criteria by 'opt = calcfc' option to obtain the reactant and product along the reaction coordinate.

Additional geometry optimizations for key transition states were carried out at the M06 functional.[15] Single point energies were calculated at the $SMD_{(Toluene)}$/M06/6-31G**,LANL2DZ(Pd)//B3LYP/6-31G**,LANL2DZ(Pd) level of theory. The effect of a solvent continuum, in toluene, was evaluated using the Cramer−Truhlar continuum solvation model that employs quantum mechanical charge density of solutes, designated as SMD.[16] The zero-point vibrational energy (ZPVE), thermal, and entropic corrections obtained at 298.15 K and 1 atm pressure derived from the gas phase computations have been applied to the "bottom-of-the-well" energies obtained from the single-point energy evaluations in the solvent phase to estimate the Gibbs free energies of solutes in the condensed phase. The discussions are presented using the M06/6-31G**,LANL2DZ-(Pd) level of theory.

The *Activation Strain* model is applied to examine the origin of the energy difference between the stereodetermining TSs for catalyst **III** with both active species **1a** and **2**.[17] In the distortion-interaction model, the activation barrier ($\Delta E^{\ddagger}$) is considered as arising due to the destabilizing distortion in the reacting partners ($\Delta E^{\ddagger}_{d}$) upon going from their respective ground state geometries to that in the transition states and the stabilizing interaction energy between these distorted fragments ($\Delta E^{\ddagger}_{i}$) in the TS geometry. The distortion energies and the interaction energies are compared to the lowest energy TS.

dx.doi.org/10.1021/jo501322v | J. Org. Chem. 2014, 79, 7600−7606

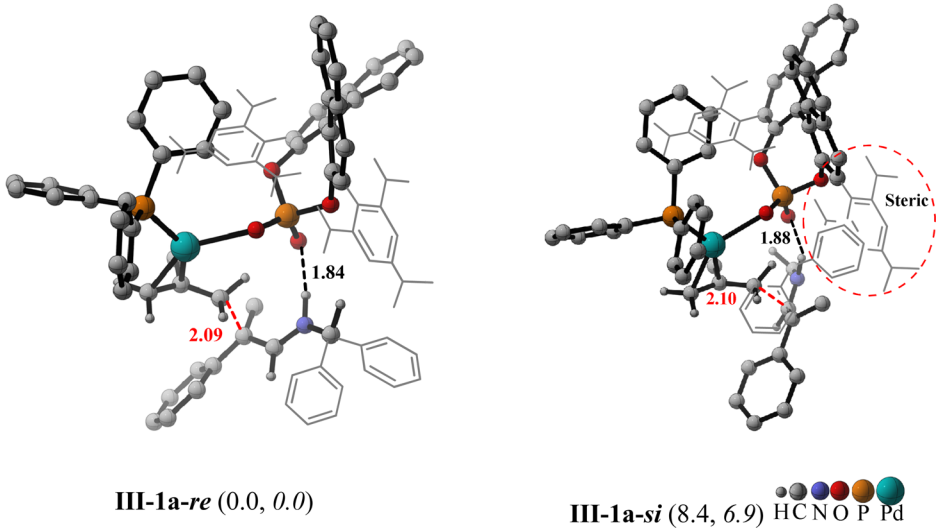

Figure 1. Optimized geometries of the lower energy transition states for catalyst **III** with active species **1a** (ligand mode). The relative free energies in the gas phase (kcal/mol) and in the condensed phase are provided in parentheses using, respectively, normal and italic fonts.

RESULTS AND DISCUSSION

Chiral phosphoric acids **I** and **III** are considered as the Brønsted acids in the present study (Scheme 1). The role of different active species **1a**, **1b**, and **2**, which differ in the number of phosphine ligands on Pd, is examined (Scheme 2(ii)). While palladium bis-phosphine **2** is the most commonly proposed active species,[4,6] some recent evidence point to the presence of a mixed phosphine-phosphate **1** as the active species as well.[18] For instance, a crystal structure of Pd bound TRIP (**III**) anion has been recently reported.[6b] The evidence for a mono-phosphine **1b** as the active species comes form another recent study, wherein a cationic species like **1b** has been detected.[6g] In yet another interesting report, a TRIP-Pd-allyl complex has not only been detected as the catalytic species but also used directly as a catalyst by its separate inclusion.[19] In view of this literature precedence, we have computed the energies of such active species to ascertain their relative potential as the catalytic active species. The relative energies provided in Scheme 2 suggest that bis(triphenylphosphine)-Pd-π-allyl complex **2** is more likely the preferred candidate to remain as the active species. However, displacement of a phosphine by a phosphate ligand (leading to **1a**) cannot be fully discounted. Hence, we have separately examined the stereocontrolling transition states with all of the three active species. A comparison between the stoichiometrically different **1a**, **1b**, and **2** is enabled by appropriate mass balance by way of including the energy of triphenylphosphine to **1a** and **1b**.

The emphasis is placed on the stereocontrolling C−C bond formation wherein the enamine (derived from benzylaldehyde and benzhydryl amine) adds to the Pd-π-allyl complex. First, the stereocontrolling TSs with **1a**, **1b**, and **2** in the case of catalyst **I** is examined.[20] A thorough conformational sampling is performed with catalyst **I** to identify all key lower energy conformers.[21]

Insights gained through the analysis of the stereocontrolling TSs for catalyst **I** is now extended to the experimentally known most successful catalyst **III**, wherein the 3,3′ positions on the binol are occupied by 2,4,6-triisopropylphenyl groups. The TSs with active species with one triphenylphosphine ligand on Pd (**1a** and **1b**) are compared first. The lower energy diastereomeric TSs for catalyst **III** with active species **1a** (ligand mode) are given in Figure 1.[22] The corresponding TS with active species **1b** is found to be 7.7 kcal/mol higher in energy than that with **1a**. The enantioselectivity calculated using the active species **1a** is >99%, which is in agreement with the experimental value of 88%. A closer perusal of the ee-determining TSs **III-1a-*re*** and **III-1a-*si*** indicates that in the lower energy TS **III-1a-*re*** the bulkier diphenyl methyl group of the enamine moiety remains away from the substituents at the 3,3′ position of the binol as shown in Figure 1. In the higher energy TS **III-1a-*si*** an enhanced steric interaction between the 3,3′ substituents of the binol and the diphenylmethyl group of the enamine is noticed (shown in red dotted circle, Figure 1). The steric bulk at the binol 3/3′ positions in conjunction with that of the incoming enamine is responsible for the enantioselectivity in active species **1a**. The *Activation Strain analysis* conveys that the lower energy TS, **III-1a-*re***, has 8.7 kcal/mol higher interaction energy and 0.3 kcal/mol lower distortion than in TS **III-1a-*si***. Thus, the stereoinduction is primarily controlled by the favorable interaction between TRIP-Pd-allyl complex and the enamine than the unfavorable distortion in each fragment of the TS.

The role of active species **2** comprising two triphenylphosphines on Pd is examined next.[23] In **2**, only the counterion mode is viable for the chiral phosphate due to the large spacial spread of the bulky triphenylphosphines. The most important aspect pertaining to the counterion TS model **2** is that it is energetically lower than the corresponding TSs with both active species **1a** and **1b**. For example, the most preferred TSs involving the *re* face addition of the enamine to Pd-π-allyl species for catalyst III with active species **2** is 13 kcal/mol lower in energy than that with **1a** and as much as 20 kcal/mol lower than that with active species **1b**. On the basis of the relative energies of (i) the active species itself (Scheme 2) and (ii) the stereocontrolling C−C bond formation TSs, it is evident that bis(triphenylphosphine)-Pd-allyl (**2**) holds the key to the enantioselectivity of the title reaction. The chiral counterion should therefore be regarded as inducing chirality through an outer-sphere interaction.

After establishing the nature of the active species in the stereocontrolling C−C bond formation step, we have examined the factors that govern chiral induction. For catalyst **III**, with **2**

dx.doi.org/10.1021/jo501322v | *J. Org. Chem.* 2014, 79, 7600−7606

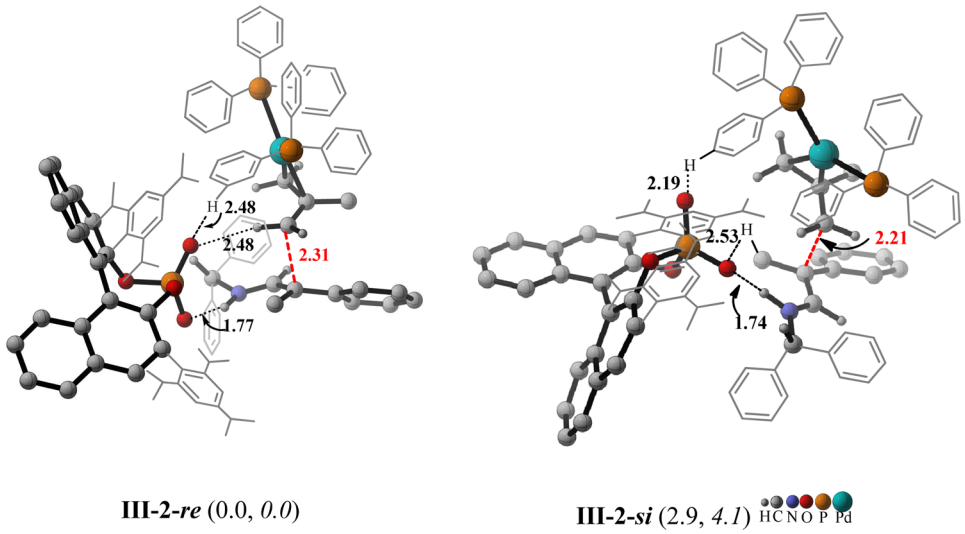

Figure 2. Optimized geometries of the lower energy TSs for catalyst **III** with active species **2**. The relative free energies in the gas phase (kcal/mol) and in the condensed phase are provided in parentheses using, respectively, normal and italic fonts.

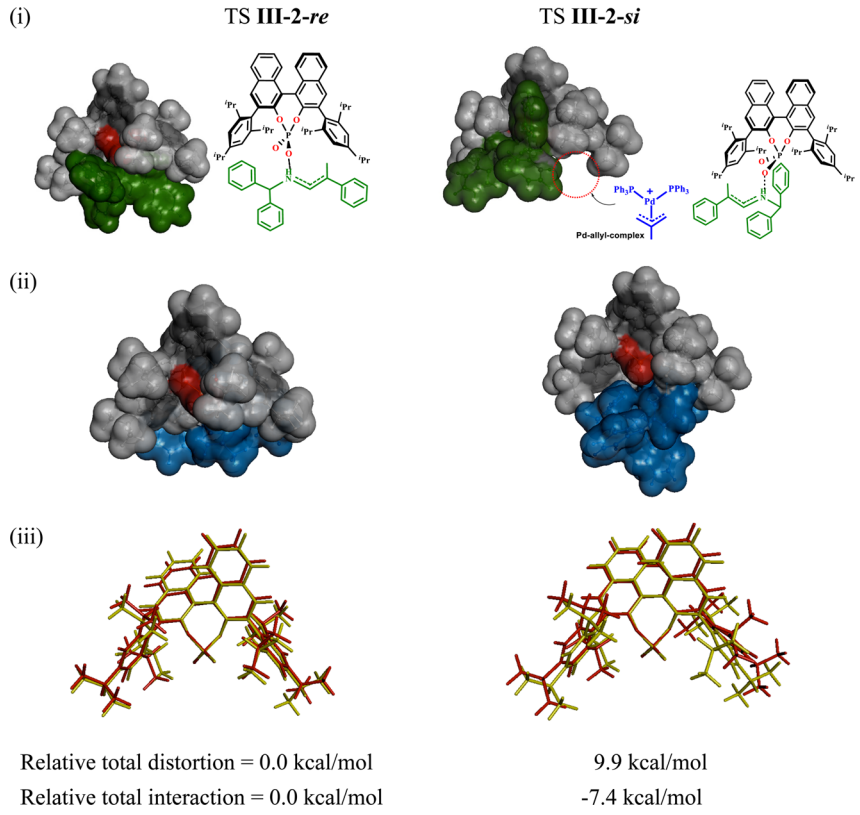

Figure 3. Space filling 3D models derived from TS geometries (**III-2-*re*** and **III-2-*si***) depicting the chiral counterion (i) with only the enamine (green) fragment and (ii) with only the Pd-allyl substrate (blue). (iii) Superimposed geometries of chiral counterion (yellow) with the distorted counterion backbone (red) in the diastereomeric TSs **III-2-*re*** and **III-2-*si***.

as the active species, the energy difference between the diastereomeric TSs is found to be 2.9 kcal/mol.[24] The predicted ee of 99% in favor of the *R* enantiomer is in excellent agreement, both in terms of extent and sense of slectivity, with the experimental value of 88%. The optimized TS geometries convey some vital details that help rationalize this energy difference (Figure 2). The Pd···$O_{phosphate}$ distances are greater than 4.5 Å in both of the diastereomeric TSs, indicating the lack of any direct interaction between Pd and the phosphate counterion. The chiral phosphate counterion is identified as being held by multiple interactions such as (i) an ionic hydrogen bond[25] between the enamine N–H and the phosphate oxygen (1.77 Å in **III-2-*re*** and 1.74 Å in **III-2-*si***) and (ii) C–H···O interactions[26] between bis(triphenylphosphine)-Pd-π-allyl moiety and the phosphate oxygen. Thus, it is evident that the positioning of the activated substrate (allyl and enamine) in the TSs is facilitated by a network of noncovalent interactions offered by the chiral phosphate counterion. These

dx.doi.org/10.1021/jo501322v | J. Org. Chem. 2014, 79, 7600–7606

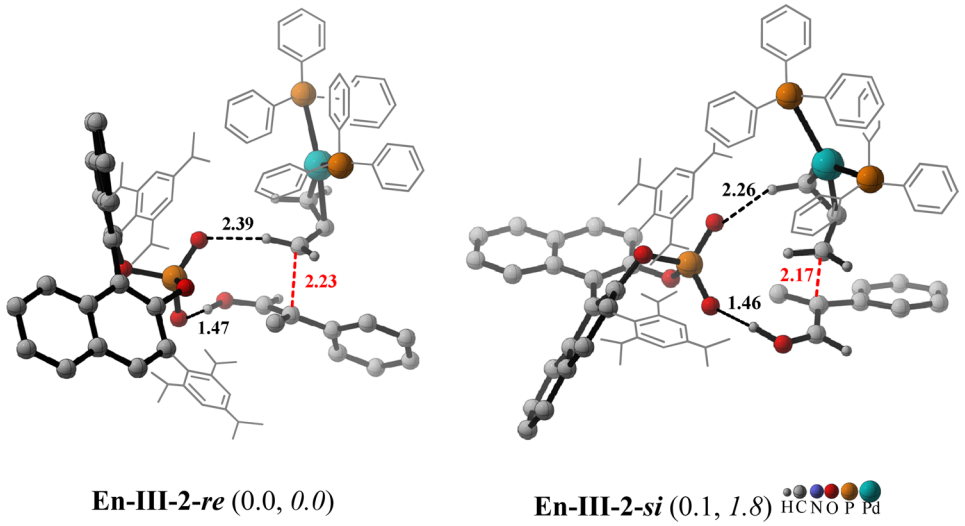

Figure 4. Optimized geometries of the lower energy TSs for catalyst **III** with active species **2** for the enol pathway. The relative free energies in the gas phase (kcal/mol) and in the condensed phase are provided in parentheses using, respectively, normal and italic fonts.

insights support that the enantioselectivity is counterion-controlled as opposed to the traditional ligand-guided catalysis. Another TS model wherein the ionic H-bond (N−H···$O_{phosphate}$) distance is 2.16 Å, as opposed to 1.77 Å as noted in TS **III-2-*re***, is found to be about 10 kcal/mol higher than TS **III-2-*re***, underscoring the importance of the pivotal H-bonding between the enamine and the chiral counterion.[27]

The above-mentioned weak interactions contribute to how well the reactants fit in the chiral space of the phosphate counterion. It can be noticed from the space filling models derived for the stereocontrolling TSs (Figure 3(i)) that in the lower energy TS **III-2-*re*** the enamine moiety (shown in green) fits very well in the chiral space. This further implies that the direction of approach of the Pd-π-allyl fragment would have to be from the rear side.[28] However, in the higher energy TS **III-2-*si***, wherein the *si* face of the enamine is exposed to the Pd-π-allyl fragment, the substrate fit appears less efficient, leaving an empty space as depicted using the red dotted-line circle. This empty space is occupied by the Pd-π-allyl complex (shown in blue). In other words, in the higher energy TS **III-2-*si*** both enamine and Pd-π-allyl moiety are forced to share the chiral space. Such an arrangement is likely to cause increased distortion of the chiral counterion. To quantify the extent of distortion caused by induced fit of the substrates and its role on the origin of stereoinduction, activation strain analysis is carried out on the stereodetermining TSs.

The geometric distortion of the substrates and the catalysts are estimated by comparing the energy of the respective distorted structures as in the transition state with that of the native undistorted ground state geometry. Interestingly, the largest distortion is seen in the chiral phosphate counterion.[29] The overlaid images (Figure 3(iii)) of the phosphate backbone of the initial undistorted (yellow) and distorted TS (red) structures evidently suggest that the extent of distortion in the higher energy TS **III-2-*si*** is more than that in TS **III-2-*re***. The difference in the distortion in the counterion with respect to the corresponding undistorted geometry in these TSs is ascertained using the RMSD values. The distortion of **III-2-*re*** and **III-2-*si*** are estimated to be 0.034 and 0.057 Å, respectively. In the calculated total distortion of 9.9 kcal/mol in TS **III-2-*si***, 7.3 kcal/mol is traced to the distortion in the phosphate counterion. The major contributing factor to this distortion stems from the reorganization of the binol 3,3′ aryl groups. Quite noteworthy is the net stabilization through favorable interaction between the reacting partners (Pd-allyl complex, phosphate counterion, and enamine), which is 7.4 kcal/mol lower in TS **III-2-*re*** than that in **III-2-*si***. Thus, the relative energies of the stereocontrolling TSs are decided primarily by the extent of distortion in the chiral catalyst that outweighs the effect of interaction.

Another interesting observation relating to the title reaction is that the products are formed in good yield, albeit with no enantioselectivity, even in the absence of benzhydrylamine. Under such conditions, in place of enamine, the enol tautomer of benzylaldehyde should be regarded as responsible for the C−C bond formation with Pd-π-allyl complex.[30] Due to the low steric bulk on the enol, the computed energy difference between the diastereomeric TSs is found to be very small, leading to hardly any enantioselectivity, which is in line with the experimental value of 10%. The optimized geometries are provided in Figure 4. In the absence of bulkier enamines, such as the one derived using benzhydrylamine, enhancing the enantioselectivity would demand greater steric bulk at the chiral moiety.[6g]

■ CONCLUSION

In summary, the origin of enantioselectivity in a cooperative triple catalytic reaction between an aldehyde and allylic alcohol in the presence of a chiral phosphoric acid is established. In the most preferred transition state for the stereocontrolling C−C bond formation between the substrates (activated in the form of an enamine and a bis(triphenylphosphine)-Pd-π-allyl complex), the chiral phosphate ion is found to remain as a counterion. The study provides the first transition state model for counterion-directed enantioselective generation of a quaternary chiral carbon. The chirality transfer is identified as taking place through an ionic H-bond between the enamine and the chiral phosphate counterion in addition to a network of weak noncovalent interaction with the Pd-π-allyl complex. This is in contrast to the conventional models wherein the chiral ligand is directly bound to the transition metal. The differences in the distortion of the chiral counterion backbone between the

dx.doi.org/10.1021/jo501322v | J. Org. Chem. 2014, 79, 7600−7606

diastereomeric transition states contribute to their vital energy separation that is responsible for the observed enantioselectivity. Modifications of substituents on the enamine as well as the 3,3′ positions of the BINOL-phosphoric acid could offer leads toward broadening the scope of asymmetric Tsuji−Trost allylation and other related reactions using a counterion strategy.

■ ASSOCIATED CONTENT

Supporting Information

Optimized geometries for all stationary points, computed energetics, and additional information regarding alternative higher energy pathways. This material is available free of charge via the Internet at http://pubs.acs.org.

■ AUTHOR INFORMATION

Corresponding Author

*E-mail: sunoj@chem.iitb.ac.in.

Notes

The authors declare no competing financial interest.

■ ACKNOWLEDGMENTS

Research funding from BRNS (Mumbai) under the basic sciences scheme, generous computing time from IIT Bombay computer center, as well as National Nanotechnology Infrastructure Network (NNIN) at Michigan are gratefully acknowledged. Senior research fellowship to G.J. from CSIR (New Delhi) is acknowledged.

■ REFERENCES

(1) (a) Desimoni, G.; Faita, G.; Jørgenson, K. A. *Chem. Rev.* **2011**, *111*, PR284. (b) Hawner, C.; Alexakis, A. *Chem. Commun.* **2010**, *46*, 7295. (c) *Comprehensive Asymmetric Catalysis* and Supplements 1 and 2; Jacobsen, E. N.; Pfaltz, A.;Yamamoto, H., Eds.; Springer: New York, 1999, 2004. (d) Trost, B. M.; Crawley, M. L. *Chem. Rev.* **2003**, *103*, 2921. (e) Lu, Z.; Ma, S.-M. *Angew. Chem., Int. Ed.* **2008**, *47*, 258.

(2) (a) Knowles, R. R.; Jacobsen, E. N. *Proc. Natl. Acad. Sci. U.S.A.* **2010**, *107*, 20678. (b) Doyle, A. G.; Jacobsen, E. N. *Chem. Rev.* **2007**, *107*, 5713. (c) Lacour, J.; Moraleda, D. *Chem. Commun.* **2009**, 7073. (d) Brak, K.; Jacobsen, E. N. *Angew. Chem., Int. Ed.* **2013**, *52*, 534. (e) Raynal, M.; Ballester, P.; Vidal-Ferran, A.; van Leeuwen, P. W. N. M. *Chem. Soc. Rev.* **2014**, *43*, 1660.

(3) (a) Xu, H.; Zeund, S. J.; Woll, M. G.; Tao, Y.; Jacobsen, E. N. *Science* **2010**, *327*, 986. (b) Rueping, M.; Koenigs, R. M.; Atodiresei, I. *Chem.—Eur. J.* **2010**, *16*, 9350. (c) Shao, Z.; Zhang, H. *Chem. Soc. Rev.* **2009**, *38*, 2745. (d) Paull, D. H.; Abraham, C. J.; Scerba, M. T.; Alden-Danforth, E.; Lectka, T. *Acc. Chem. Res.* **2008**, *41*, 655. (e) Zhong, C.; Shi, X. *Eur. J. Org. Chem.* **2010**, 2999.

(4) (a) Phipps, R. J.; Hamilton, G. L.; Toste, F. D. *Nat. Chem.* **2012**, *4*, 603 and references therein. (b) Mahlau, M.; List, B. *Angew. Chem., Int. Ed.* **2013**, *52*, 518. (c) Avila, E. P.; Amarante, G. W. *ChemCatChem.* **2012**, *4*, 1713.

(5) For select examples of organocatalysis, see: (a) Mayer, S.; List, B. *Angew. Chem., Int. Ed.* **2006**, *45*, 4193. (b) Wang, X.; List, B. *Angew. Chem., Int. Ed.* **2008**, *47*, 1119. (c) Hamilton, G. L.; Kanai, T.; Toste, F. D. *J. Am. Chem. Soc.* **2008**, *130*, 14984. (d) García-García, P.; Lay, F.; García-García, P.; Rabalakos, C.; List, B. *Angew. Chem., Int. Ed.* **2009**, *48*, 4363. (e) Terada, M.; Tanaka, H.; Sorimachi, K. *J. Am. Chem. Soc.* **2009**, *131*, 3430. (f) Rueping, M.; Uria, U.; Lin, M.-Y.; Atodiresei, I. *J. Am. Chem. Soc.* **2011**, *133*, 3732. (g) Čorić, I.; List, B. *Nature* **2012**, *483*, 315. For reviews on Brønsted acid catalysis, see: (h) Akiyama, T. *Chem. Rev.* **2007**, *107*, 5744. (i) Terada, M. *Synthesis* **2010**, 1929.

(6) For examples of Pd-catalyzed reactions, see: (a) Mukherjee, S.; List, B. *J. Am. Chem. Soc.* **2007**, *129*, 11336. (b) Jiang, G.; Halder, R.; Fang, Y.; List, B. *Angew. Chem., Int. Ed.* **2011**, *50*, 9752. (c) Chai, Z.; Rainey, T. J. *J. Am. Chem. Soc.* **2012**, *134*, 3615. (d) Guo, B.; Schwarzwalder, G.; Njardarson, J. T. *Angew. Chem., Int. Ed.* **2012**, *51*, 5675. (e) Ohmatsu, K.; Ito, M.; Kunieda, T.; Ooi, T. *Nat. Chem.* **2012**, *4*, 473. (f) Alper, H.; Hamel, N. *J. Am. Chem. Soc.* **1990**, *112*, 2803. (g) Tao, Z.-L.; Zhang, W.-Q.; Chen, D.-F.; Adele, A.; Gong, L.-Z. *J. Am. Chem. Soc.* **2013**, *135*, 9255. For metals other than Pd, see: (h) Hamilton, G. L.; Kang, E. J.; Mba, M.; Toste, F. D. *Science* **2007**, *317*, 496. (i) Liao, S.; List, B. *Angew. Chem., Int. Ed.* **2010**, *49*, 628. (j) Zbieg, J. R.; Yamaguchi, E.; McInturff, E. L.; Krische, M. J. *Science* **2012**, *336*, 324. (k) Zhou, S.; Fleischer, S.; Junge, K.; Beller, M. *Angew. Chem., Int. Ed.* **2011**, *50*, 5120. (l) Llewellyn, D. B.; Adamson, D.; Arndtsen, B. A. *Org. Lett.* **2000**, *2*, 4165. For a review on metal phosphates, see: (m) Parra, A.; Reboredo, S.; Castroa, A. M. M.; Alemán, J. *Org. Biomol. Chem.* **2012**, *10*, 5001.

(7) Jiang, G.; List, B. *Angew. Chem., Int. Ed.* **2011**, *50*, 9471.

(8) (a) Fleischmann, M.; Drettwan, D.; Sugiono, E.; Rueping, M.; Gschwind, R. M. *Angew. Chem., Int. Ed.* **2011**, *50*, 6364. (b) Simón, L.; Goodman, J. M. *J. Am. Chem. Soc.* **2008**, *130*, 8741.

(9) A few studies aimed at understanding the nature of the chiral species in metal catalysis other than Pd have been reported. See: (a) Nguyen, B. N.; Adrio, L. A.; Barreiro, E. M.; Brazier, J. B.; Haycock, P.; Hii, K. K.; Nachtegaal, M.; Newton, M. A.; Szlachetko, J. *Organometallics* **2012**, *31*, 2395. (b) Barbazanges, M.; Augé, M.; Moussa, J.; Amouri, H.; Aubert, C.; Desmarets, C.; Fensterbank, L.; Gandon, V.; Malacria, M.; Ollivier, C. *Chem.—Eur. J.* **2011**, *17*, 13789. (c) Xu, B.; Zhu, S.-F.; Xie, X.-L.; Shen, J.-J.; Zhou, Q.-L. *Angew. Chem., Int. Ed.* **2011**, *50*, 11483. For other studies on counterions, see: (d) Kim, J. H.; Park, S.-W.; Park, S. R.; Lee, S.; Kang, E. J. *Chem.—Asian J.* **2011**, *6*, 1982. (e) Wang, M.-Z.; Zhou, C.-Y.; Guo, Z.; Wong, E. L.-M.; Wong, M.-K.; Che, C.-M. *Chem.—Asian J.* **2011**, *6*, 812. (f) Kovács, G.; Ujaque, G.; Lledós, A. *J. Am. Chem. Soc.* **2008**, *130*, 853. (g) Bolm, C.; Martin, M.; Gescheidt, G.; Palivan, C.; Stanoeva, T.; Bertagnolli, H.; Feth, M.; Schweiger, A.; Mitrikas, G.; Harmer, J. *Chem.—Eur. J.* **2007**, *13*, 1842. (h) Fraile, J. M.; Garcìa, J. I.; Gil, M. J.; M.-Merino, V.; Mayoral, J. A.; Salvatella, L. *Chem.—Eur. J.* **2004**, *10*, 758.

(10) (a) Shinisha, C. B.; Sunoj, R. B. *J. Am. Chem. Soc.* **2010**, *132*, 12319. (b) Sharma, A. K.; Sunoj, R. B. *Angew. Chem., Int. Ed.* **2010**, *49*, 6373. (c) Sharma, A. K.; Sunoj, R. B. *Chem. Commun.* **2011**, *47*, 5759. (d) Jindal, G.; Sunoj, R. B. *Chem.—Eur. J.* **2012**, *18*, 7045. (e) Kuniyil, R.; Sunoj, R. B. *Org. Lett.* **2013**, *15*, 5040. (f) Jindal, G.; Sunoj, R. B. *Angew. Chem., Int. Ed.* **2014**, *53*, 4432. (g) Jindal, G.; Sunoj, R. B. *Org. Biomol. Chem.* **2014**, *12*, 2745.

(11) Frisch, M. J.; Trucks, G. W.; Schlegel, H. B.; Scuseria, G. E.; Robb, M. A.; Cheeseman, J. R.; Scalmani, G.; Barone, V.; Mennucci, B.; Petersson, G. A.; Nakatsuji, H.; Caricato, M.; Li, X.; Hratchian, H. P.; Izmaylov, A. F.; Bloino, J.; Zheng, G.; Sonnenberg, J. L.; Hada, M.; Ehara, M.; Toyota, K.; Fukuda, R.; Hasegawa, J.; Ishida, M.; Nakajima, T.; Honda, Y.; Kitao, O.; Nakai, H.; Vreven, T.; Montgomery, J. A., Jr.; Peralta, J. E.; Ogliaro, F.; Bearpark, M.; Heyd, J. J.; Brothers, E.; Kudin, K. N.; Staroverov, V. N.; Kobayashi, R.; Normand, J.; Raghavachari, K.; Rendell, A.; Burant, J. C.; Iyengar, S. S.; Tomasi, J.; Cossi, M.; Rega, N.; Millam, N. J.; Klene, M.; Knox, J. E.; Cross, J. B.; Bakken, V.; Adamo, C.; Jaramillo, J.; Gomperts, R.; Stratmann, R. E.; Yazyev, O.; Austin, A. J.; Cammi, R.; Pomelli, C.;Ochterski, J. W.; Martin, R. L.; Morokuma, K.; Zakrzewski, V. G.; Voth, G. A.; Salvador, P.; Dannenberg, J. J.; Dapprich, S.; Daniels, A. D.; Farkas, O.; Foresman, J. B.; Ortiz, J. V.; Cioslowski, J.; Fox, D. J. *Gaussian 09, Revision A.02*; Gaussian, Inc.: Wallingford, CT, 2009.

(12) (a) Hehre, W. J.; Ditchfield, R.; Pople, J. A. *J. Chem. Phys.* **1972**, *56*, 2257. (b) Hariharan, P. C.; Pople, J. A. *Theor. Chim. Acta* **1973**, *28*, 213. (c) Lee, C.; Yang, W.; Parr, R. G. *Phys. Rev. B* **1988**, *37*, 785. (d) Becke, A. D. *J. Chem. Phys.* **1993**, *98*, 5648.

(13) Hay, P. J.; Wadt, W. R. *J. Chem. Phys.* **1985**, *82*, 299.

(14) (a) Gonzalez, C.; Schlegel, H. B. *J. Chem. Phys.* **1989**, *90*, 2154. (b) Gonzalez, C.; Schlegel, H. B. *J. Phys. Chem.* **1990**, *94*, 5523.

(15) (a) Zhao, Y.; Truhlar, D. G. *Theor. Chem. Acc.* **2008**, *120*, 215. (b) Zhao, Y.; Truhlar, D. G. *Acc. Chem. Res.* **2008**, *41*, 157. (c) Zhao, Y.; Truhlar, D. G. *Org. Lett.* **2007**, *9*, 1967.
(16) Marenich, A. V.; Cramer, C. J.; Truhlar, D. G. *J. Phys. Chem. B* **2009**, *113*, 6378.
(17) (a) van Zeist, W. J.; Bickelhaupt, F. M. *Org. Biomol. Chem.* **2010**, *8*, 3118. (b) Legault, C. Y.; Garcia, Y.; Merlic, C. A.; Houk, K. N. *J. Am. Chem. Soc.* **2007**, *129*, 12664. (c) Bickelhaupt, F. M. *J. Comput. Chem.* **1999**, *20*, 114. (d) Diefenbach, A.; Bickelhaupt, F. M. *J. Phys. Chem. A* **2004**, *108*, 8460.
(18) Fristrup, P.; Ahlquist, M.; Tanner, D.; Norrby, P.-O. *J. Phys. Chem. A* **2008**, *112*, 12862.
(19) Zhang, D.; Qiu, H.; Jiang, L.; Lv, F.; Ma, C.; Hu, W. *Angew. Chem., Int. Ed.* **2013**, *52*, 13356.
(20) See Tables S3−S7, S9 and Figures S3−S8 in the Supporting Information for details on the conformational sampling.
(21) For a comparison between the geometries of **1a** and **1b**, see Figures S5 and S7 in the Supporting Information.
(22) For other conformers see, Table S8 in the Supporting Information.
(23) Various likely conformers are sampled using catalyst **I**. Additional details are provided in Table S9 in the Supporting Information.
(24) The energy difference between the stereocontrolling TSs calculation using the B3LYP-D3 functional is 5 kcal/mol.
(25) (a) In the TS, the developing iminium-like (δ^+)N−H bond makes H-bond with the phosphate better. Such ionic H-bonds typically exhibit interaction energies in the range of 5−35 kcal/mol. See: Meot-Ner (Mautner), M. *Chem. Rev.* **2012**, *112*, PR22. (b) H-bonding interactions are known to be important in Tsuji−-Trost allylation reactions. See: Butts, C. P.; Filali, E.; Lloyd-Jones, G. C.; Norrby, P.−O.; Sale, D. A.; Schramm, Y. *J. Am. Chem. Soc.* **2009**, *131*, 9945.
(26) Interestingly, phosphate ions are known to participate in strong N−H···O, O−H···O, and C−H···O hydrogen bonds. See: (a) Kumara Swamy, K. C.; Kumaraswamy, S.; Kommana, P. *J. Am. Chem. Soc.* **2001**, *123*, 12642. (b) Raymo, F. M.; Bartberger, M. D.; Houk, K. N.; Stoddart, J. F. *J. Am. Chem. Soc.* **2001**, *123*, 9264. (c) Tang, W.; Johnston, S.; Iggo, J. A.; Berry, N. G.; Phelan, M.; Lian, L.; Bacsa, J.; Xiao, J. *Angew. Chem., Int. Ed.* **2013**, *52*, 1668.
(27) The optimized geometry is provided in Figure S9 in the Supporting Information.
(28) See Figures S11 and S12 in the Supporting Information for additional illustrations of the rear side attack.
(29) Full details are provided in Table S2 and Figure S2 in the Supporting Information.
(30) For additional details, see Schemes S1−S3 in the Supporting Information.